Supporting Information

Electrochemical Wastewater Treatment with Carbon Nanotube Filters Coupled with *in situ* Generated H_2O_2

Yanbiao Liu,[a] Jianping Xie,[b] Choon Nam Ong,[a] Chad Vecitis[c] and Zhi Zhou[d,*]

a. NUS Environmental Research Institute, National University of Singapore, Singapore 117411
b. Department of Chemical and Biomolecular Engineering, National University of Singapore, Singapore 117585
c. School of Engineering and Applied Sciences, Harvard University, Cambridge, Massachusetts, United States 02138
d. Division of Environmental and Ecological Engineering and School of Civil Engineering, Purdue University, 550 Stadium Mall Drive, West Lafayette, Indiana, United States 47907

* Corresponding author: Zhi Zhou, Tel: +1-765-496-3559, E-mail: zhizhou@purdue.edu

Experimental Section

Characterization of CNT filters.

Field emission scanning electron microscopy (FESEM) analysis was conducted with a JEOL JSM-6700F electron microscope (Japan) and ImageJ (NIH) software was used to analyze obtained electron micrographs.

Measurement of H_2O_2.

The concentration of H_2O_2 was measured by the potassium iodide method.[1-3] The iodide ion (I^-) rapidly reacted with H_2O_2 to form triiodide ions (I^{3-}) that presented strong absorption at a wavelength of 352 nm (ε=26 000 $M^{-1}cm^{-1}$). The 0.2 mL sample aliquots from each experiment were mixed in a quartz cuvette containing 1.0 mL of 0.10 mol L^{-1} $C_8H_5KO_4$, and 0.75 mL solution containing 0.4 mol L^{-1} KI, 0.06 mol L^{-1} N_aOH, and 10^{-4} mol L^{-1} $(NH_4)_2M_oO_4$. The mixed solutions were allowed to stand for 2 min to stabilize before absorbance measurement. All absorbance values were measured at ambient temperature using a Shimadzu UV-1800 spectrophotometer (Japan).

Measurement of pH and DO.

Concentrations of pH and DO were measured using an Agilent 3200M multi-parameter analyzer (Singapore) and a P3211 probe and a D6111 probe, respectively. O_2 was injected into the solution before the experiment by an O_2 cylinder and N_2 was injected to provide a deoxygenated condition.

Liquid chromatography-mass spectrometry (LC-MS) analysis.

LC-MS analysis of phenol was performed on an Agilent 1290 UHPLC system (Waldbronn, Germany) coupled to 6540 quadrupole-time of flight (Q-TOF) mass

detector equipped with a dual jet stream electrospray ionization source and managed by a MassHunter workstation. The column used for the separation was an Agilent Poroshell 120 SB-C18 analytical column (2.1 × 50 mm, 2.7 μm particle size). The oven temperature was maintained at 35°C and the gradient elution involved a mobile phase consisting of (A) 0.5% acetic acid in water and (B) 0.5% acetic acid in methanol. The following solvent gradient was applied: from 10% (B) to 80% (B) between 0 – 10 min and from 80% (B) to 100% (B) between 10 – 10.1 min and then return to initial conditions between 14.1 – 18.0 min. Flow rate was set at 0.2 mL min^{-1} and 20 μL of samples was injected. The electrospray ionization-mass spectrometry (ESI-MS) was acquired in negative ion mode and the ion spray voltage and nozzle voltage was set at 3,500 V and 2,000 V, respectively. The gas temperature was set as 190 °C and nebulizer nitrogen gas flow rate was set at 45 psi. For full scan mode analysis spectra were stored from m/z 30 to 500 in centroid mode.

Calculation of H_2O_2 flux and phenol removal rate

The H_2O_2 flux was calculated by the following equation:

$$H_2O_2\ Flux = \frac{(H_2O_2)(mol/L) \times flow\ rate(L/h)}{effective\ filter\ area\ (m^2)}$$

The removal rate of phenol was calculated by the following equation:

$$Removal\ Rate = \frac{(Phenol_{in} - Phenol_{out})(mol/L) \times flow\ rate(L/h)}{effective\ filter\ area\ (m^2)}$$

FIGURES

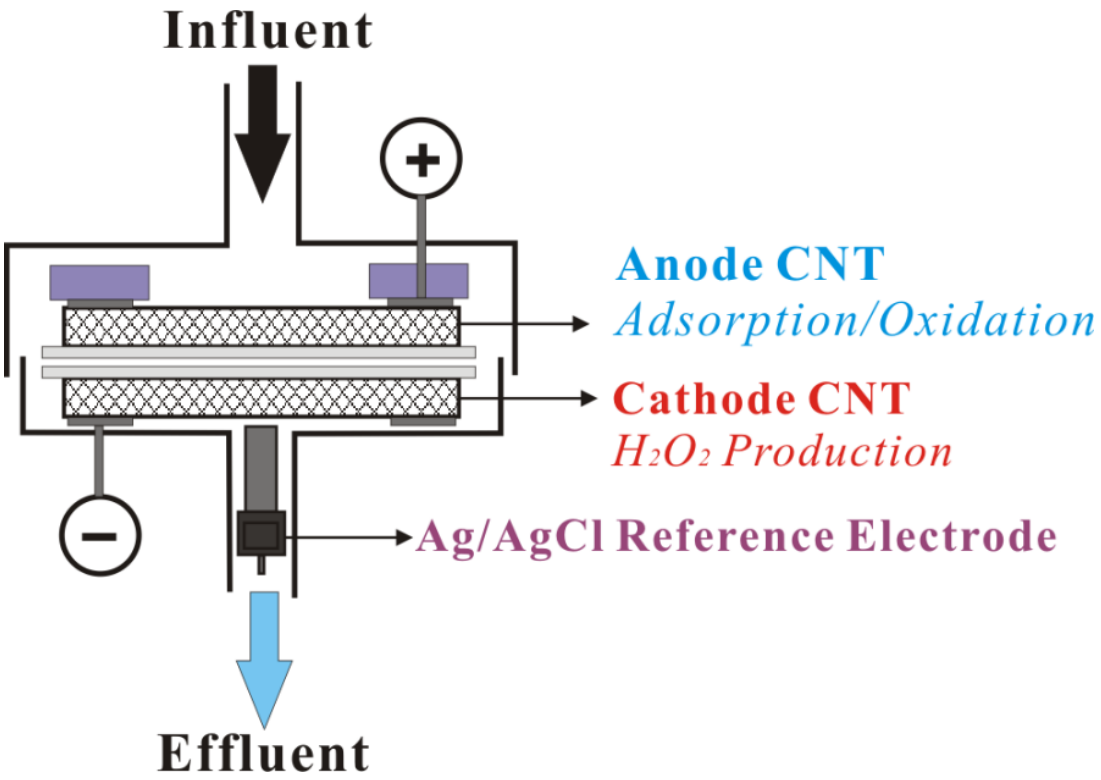

Figure S1. Schematic of the electrochemical carbon nanotube filter coupled with *in situ* generated H_2O_2.

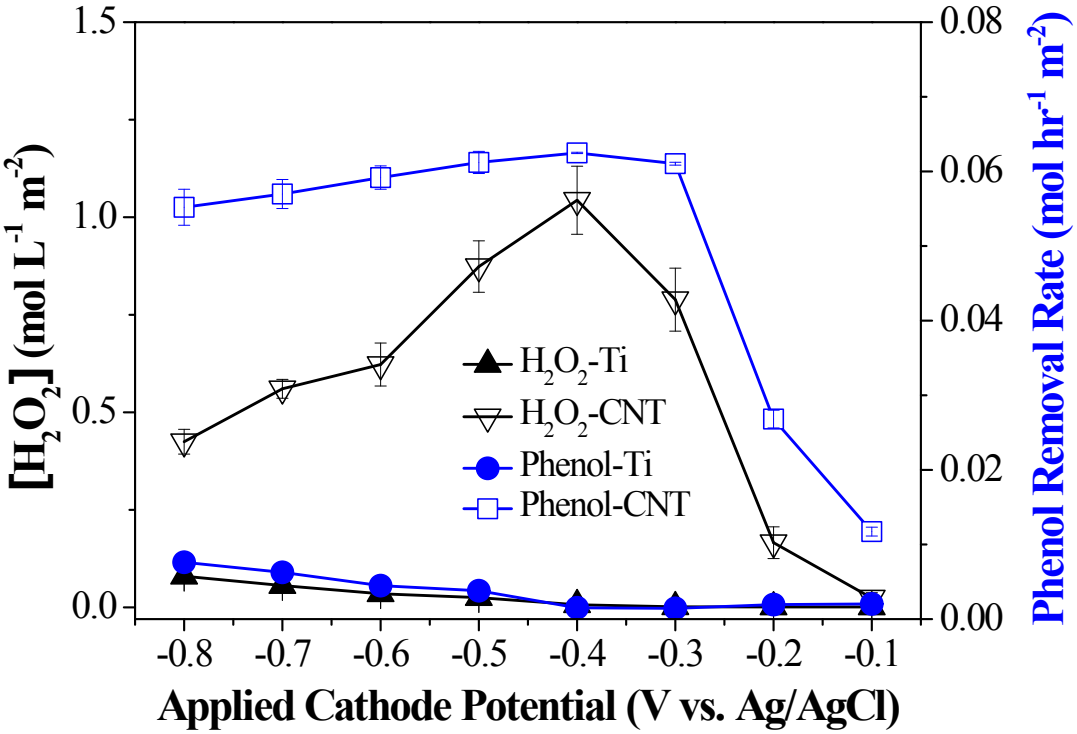

Figure S2. Effect of cathode materials on H_2O_2 flux and phenol oxidation kinetics: comparison of CNT cathode and titanium cathode. Experimental conditions: phenol flux = 2.20 mol L^{-1} m^{-2}, DO flux = 1.95 mol L^{-1} m^{-2}, [Na_2SO_4] = 10 mmol L^{-1}, flow rate = 1.5 mL min^{-1}.

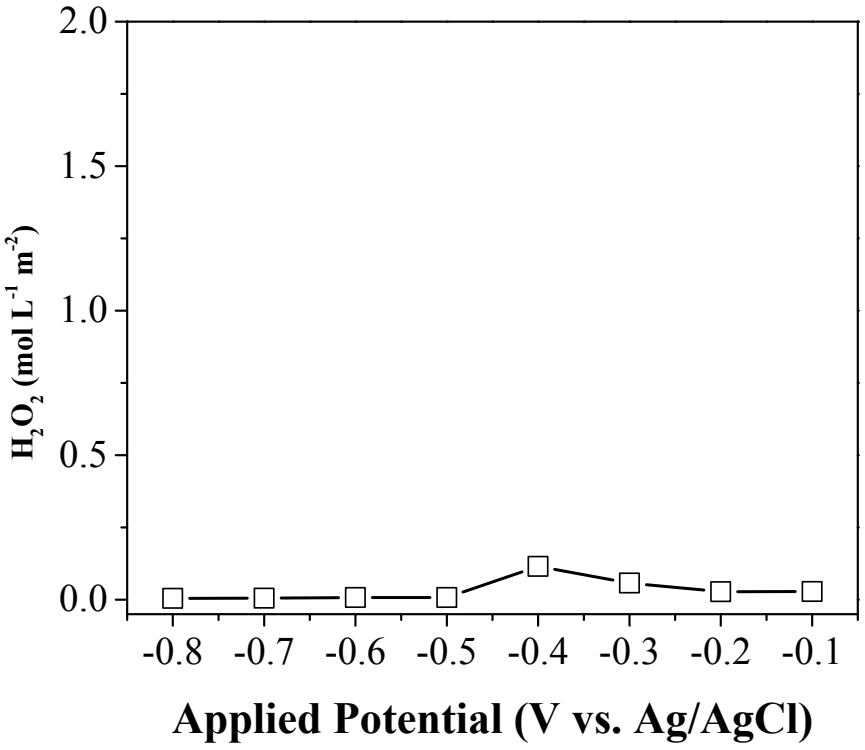

Figure S3. H_2O_2 production experiments by flowing the influent through the cathode CNT filter first. Experimental conditions: [Na_2SO_4] = 10 mmol L^{-1}, influent DO flux = 1.95 mol L^{-1} m^{-2}, flow rate = 1.5 mL min^{-1}.

Moreover, since these experiments were conducted with flow going through the anode CNT first, another control experiment was conducted at an applied potential of -0.4 V vs. Ag/AgCl by reverse the electrode order, i.e., the influent flowed through the cathode filter first. The results show that H_2O_2 flux significantly decreased by 94.2% after reversing the electrode order with a maximum H_2O_2 flux of 0.058 mol L^{-1} m^{-2}, which indicates that the cathodic produced H_2O_2 was readily oxidized at the following anode. This may also indicate the contribution of O_2 produced from anode by water oxidation to H_2O_2 production for the sequence of anode-cathode. Hence, influent was flowed through the anode filter first for all subsequent experiments.

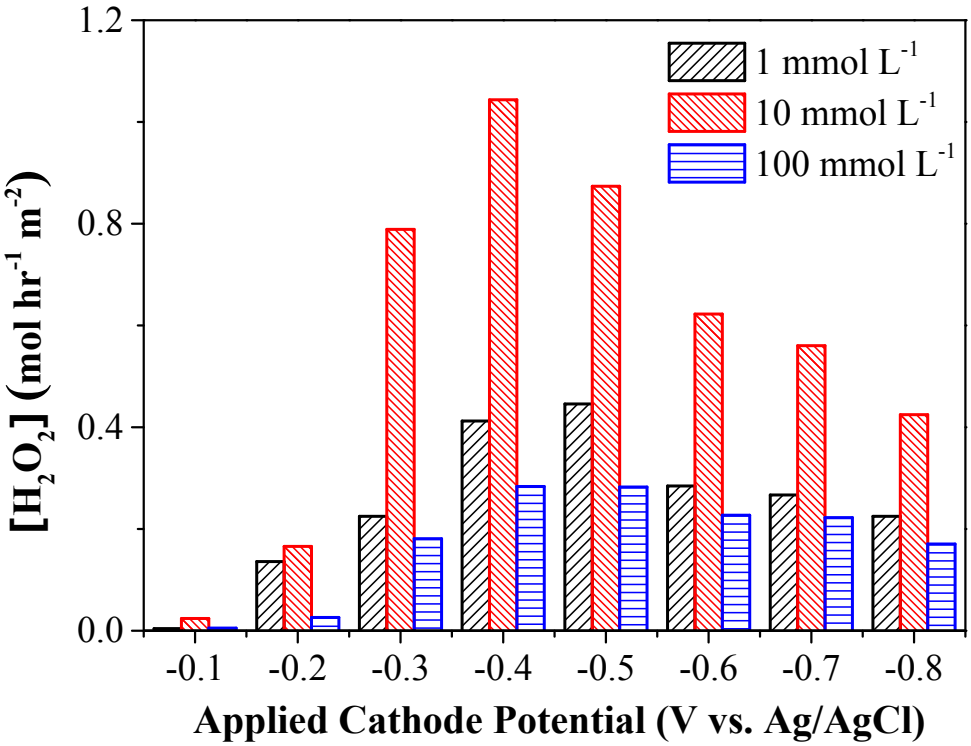

Figure S4. Effect of Na_2SO_4 concentration and applied cathode potential on H_2O_2 flux. Experimental conditions: DO flux = 1.95 mol L^{-1} m^{-2}, flow rate = 1.5 mL min^{-1}.

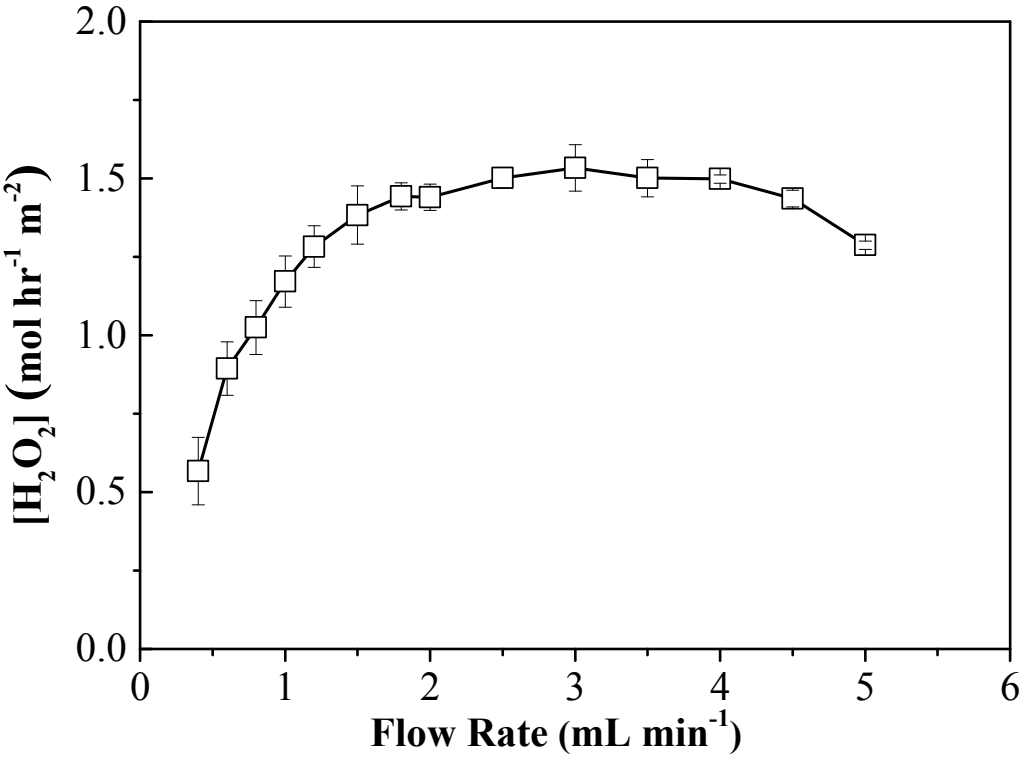

Figure S5. Electrochemical H_2O_2 flux as a function of flow rate.

The effects of flow rates on electroreduction for H_2O_2 generation were examined under optimized conditions (C-CNT-HCl, applied cathode potential of -0.4 V (vs. Ag/AgCl), influent DO flux of 1.95 mol L^{-1} m^{-2}, and [Na_2SO_4] of 10 mmol L^{-1}). At flow rates below 1.5 mL min^{-1}, H_2O_2 flux increased rapidly with increased flow rates, indicating that the filtration system was under mixed mass transfer and ORR control. Contrarily, at medium flow rate conditions (1.5-4.0 mL min^{-1}), the system became mass-transfer-limited, i.e., the electroreduction rate of O_2 was limited by the flow rate of the influent Na_2SO_4 solution throughout the cathode and subsequent replenishment of O_2 to produce H_2O_2. This was further confirmed by the stable effluent DO of 6.9±0.1 mg L^{-1} and the stable DO efficiency (i.e. the ratio of influent DO used for H_2O_2 production) of 58±2.6%. The results also indicate that Eq. 3 did not occur since that would also require further O_2 consumption and Eq. 4 likely occurred based on its reaction potential as compared with that of Eq. 5. High flow rates above 4 mL min^{-1} may be detrimental to the reduction kinetics due to greatly increased pressure within the current filtration casing, which needs further delicate engineering design to prevent such a negative effect. These results were consistent with previous studies that indicated flow rate was an important parameter influencing the kinetics within electrochemical systems, and was also consistent with the results obtained by Qiang and co-workers in a electrochemical flow-by system, which indicated that further increase in flow rate after the optimal value may not improve the H_2O_2 production.

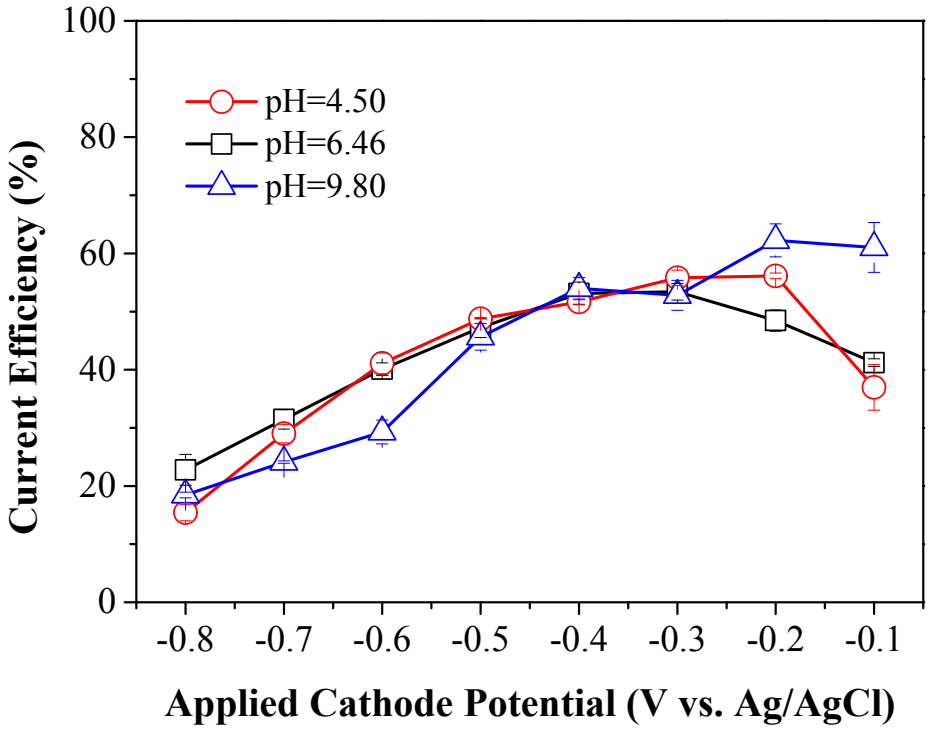

Figure S6. Current efficiency as a function of applied cathode potentials and pH.

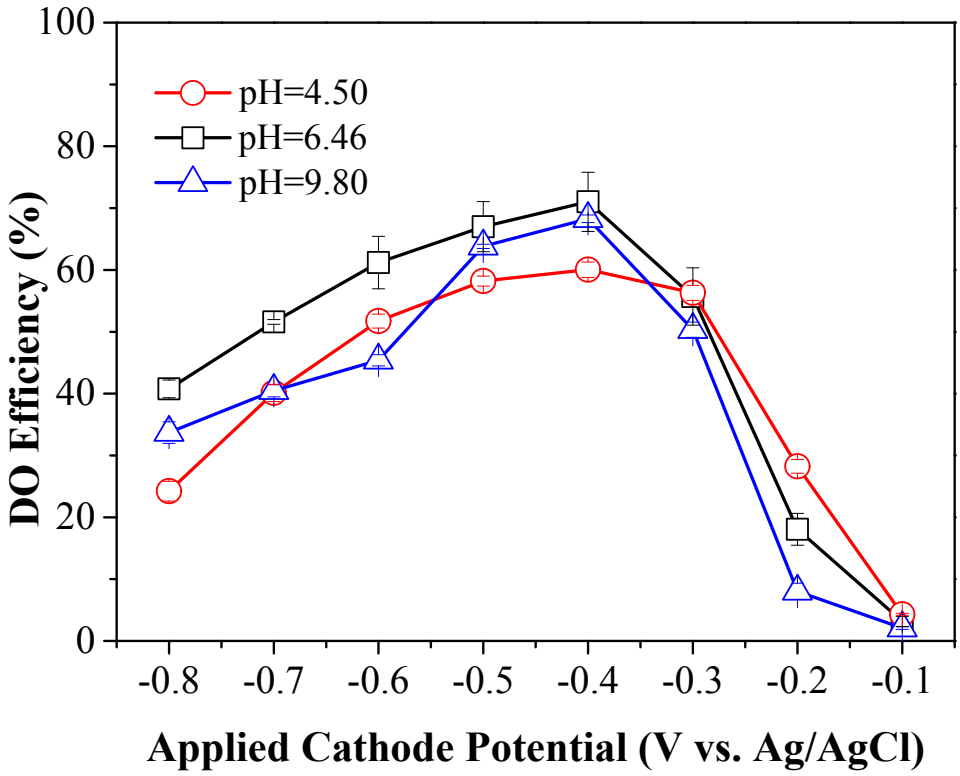

Figure S7. DO efficiency as a function applied cathode potential and pH.

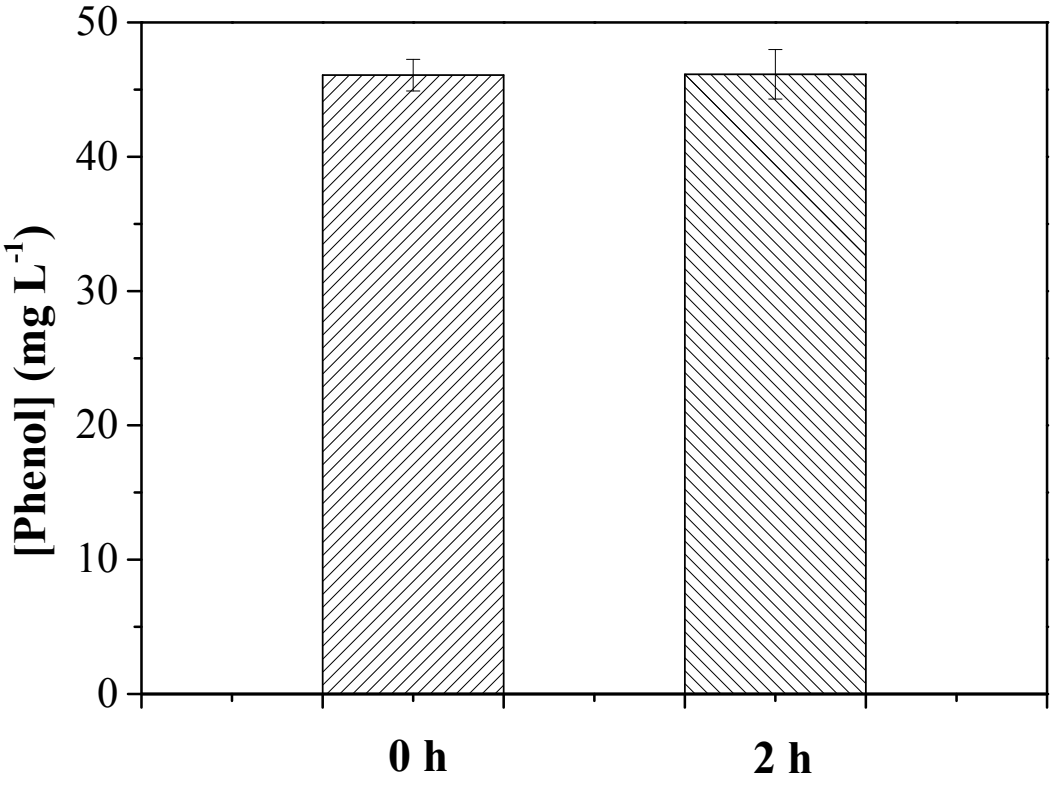

Figure S8. Change of phenol concentration before and after 2 h-exposure to 33 mg L^{-1} H_2O_2.

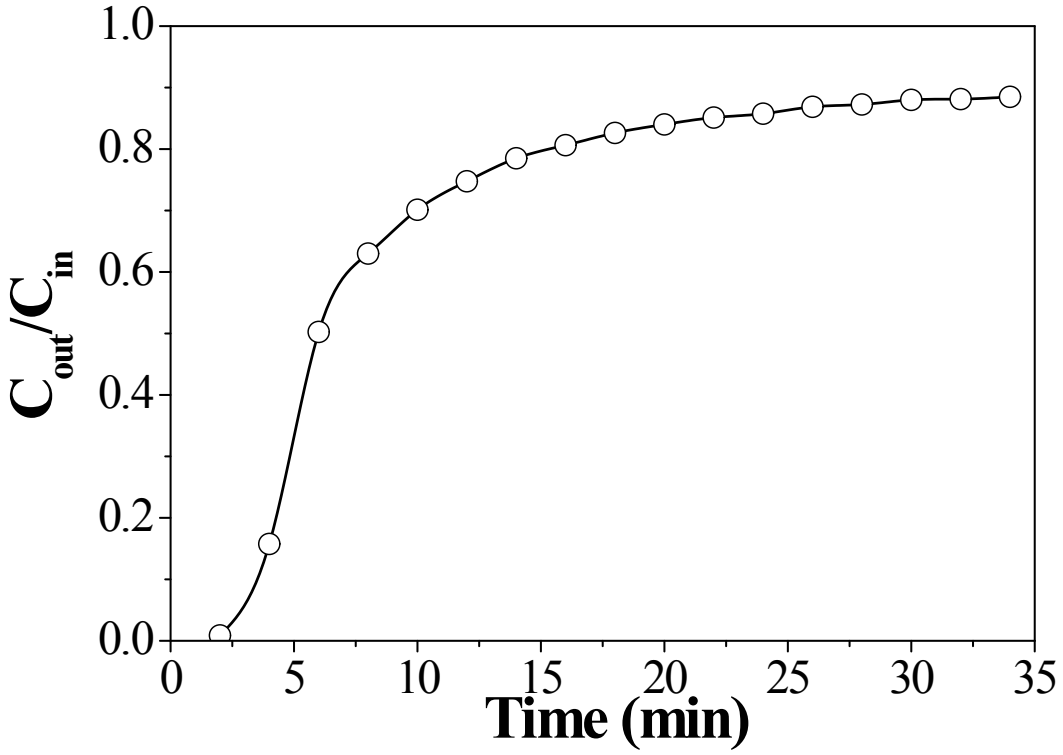

Figure S9. Breakthrough curve of 0.53 mmol L^{-1} phenol.

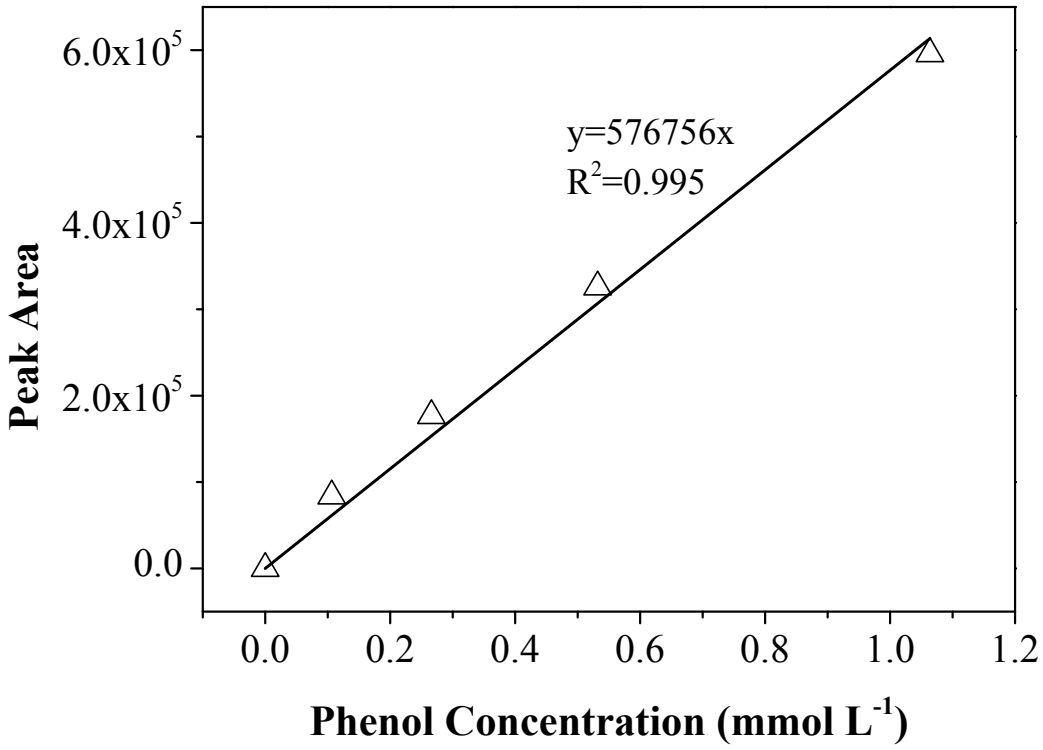

Figure S10. Calibration curve of phenol determined by HPLC-MS/QTOF.

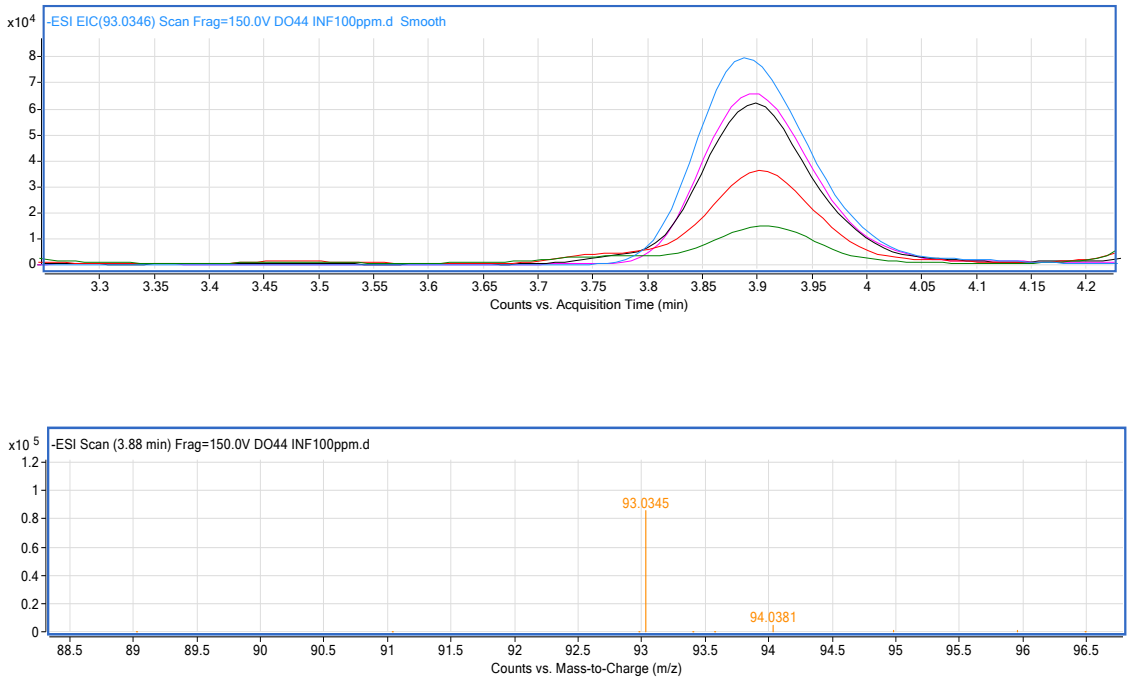

Figure S11. The extracted ion chromatogram (A) and mass spectrum (B) of m/z 93.0346 of the influent phenol and effluent samples at applied cathode potential of -0.1, -0.2, -0.3 and -0.4 V vs. Ag/AgCl. Experimental conditions: [Na_2SO_4] = 10 mmol L^{-1}, phenol flux = 2.20 mol L^{-1} m^{-2}, influent DO flux = 1.95 mol L^{-1} m^{-2}, flow rate = 1.5 mL min^{-1}.

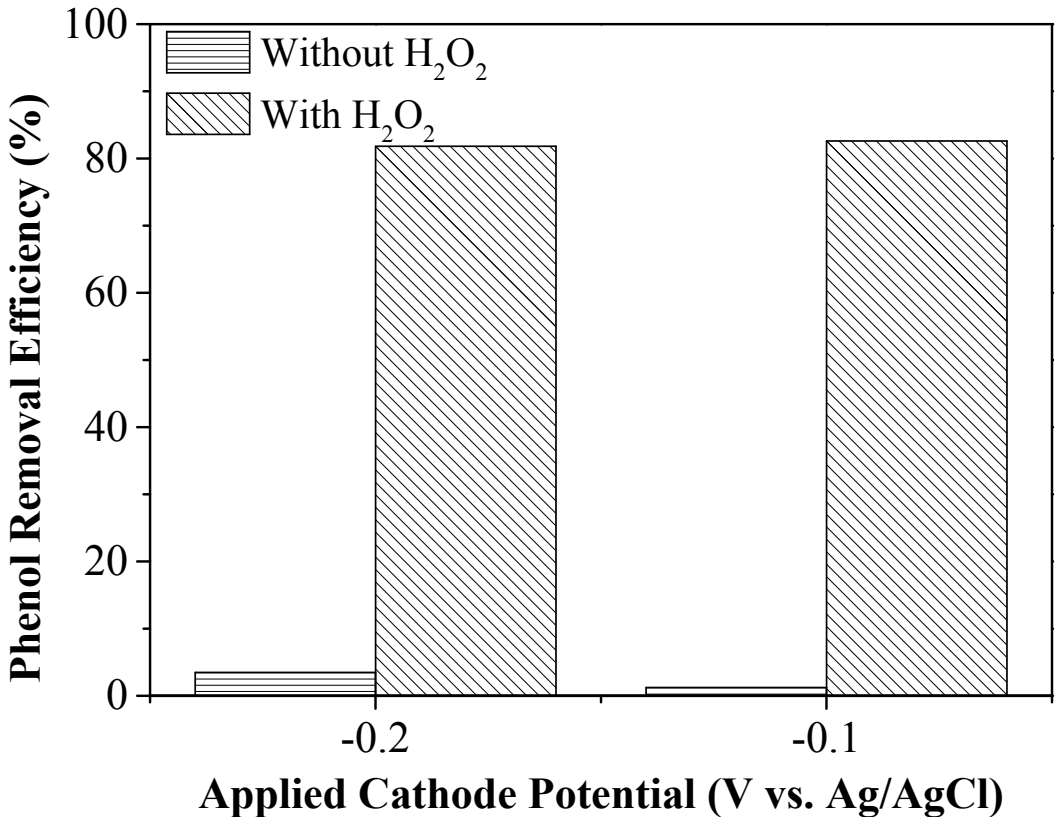

Figure S12. Comparison of phenol removal with and without the addition of H_2O_2 into the effluent. Experimental conditions: [Na_2SO_4] = 10 mmol L^{-1}, phenol flux = 2.20 mol L^{-1} m^{-2}, influent DO flux = 0 mol L^{-1} m^{-2}, flow rate = 1.5 mL min^{-1}.

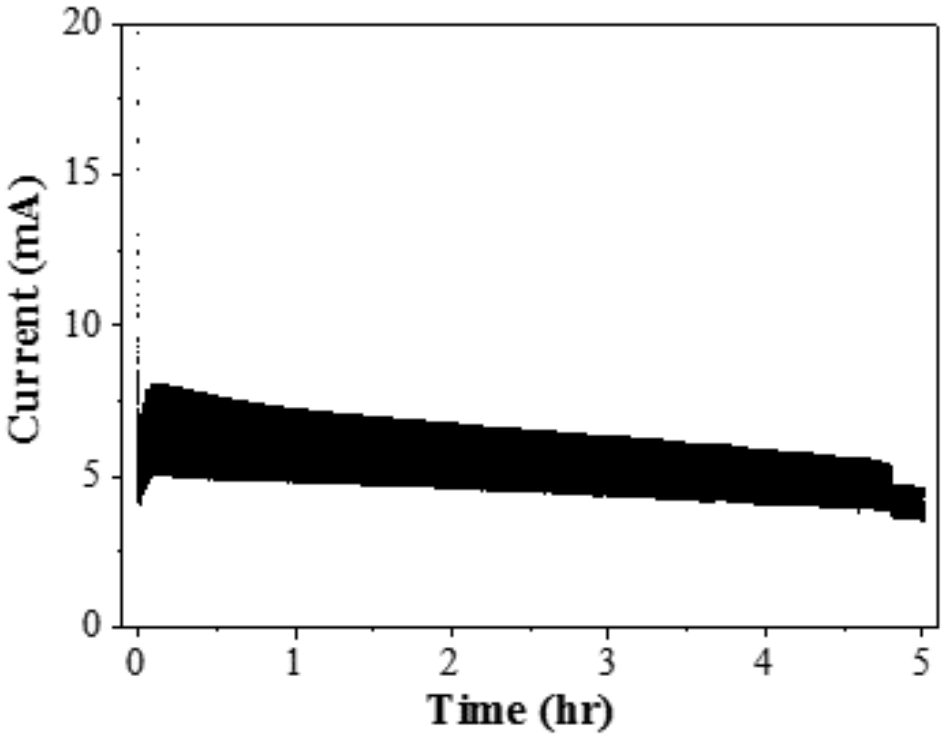

Figure S13. Change of current with time over 5 h continuous operation. Experimental conditions: $[Na_2SO_4]$ = 10 mmol L^{-1}, phenol flux = 2.20 mol L^{-1} m^{-2}, influent DO flux = 1.95 mol L^{-1} m^{-2}, flow rate = 1.5 mL min^{-1}.

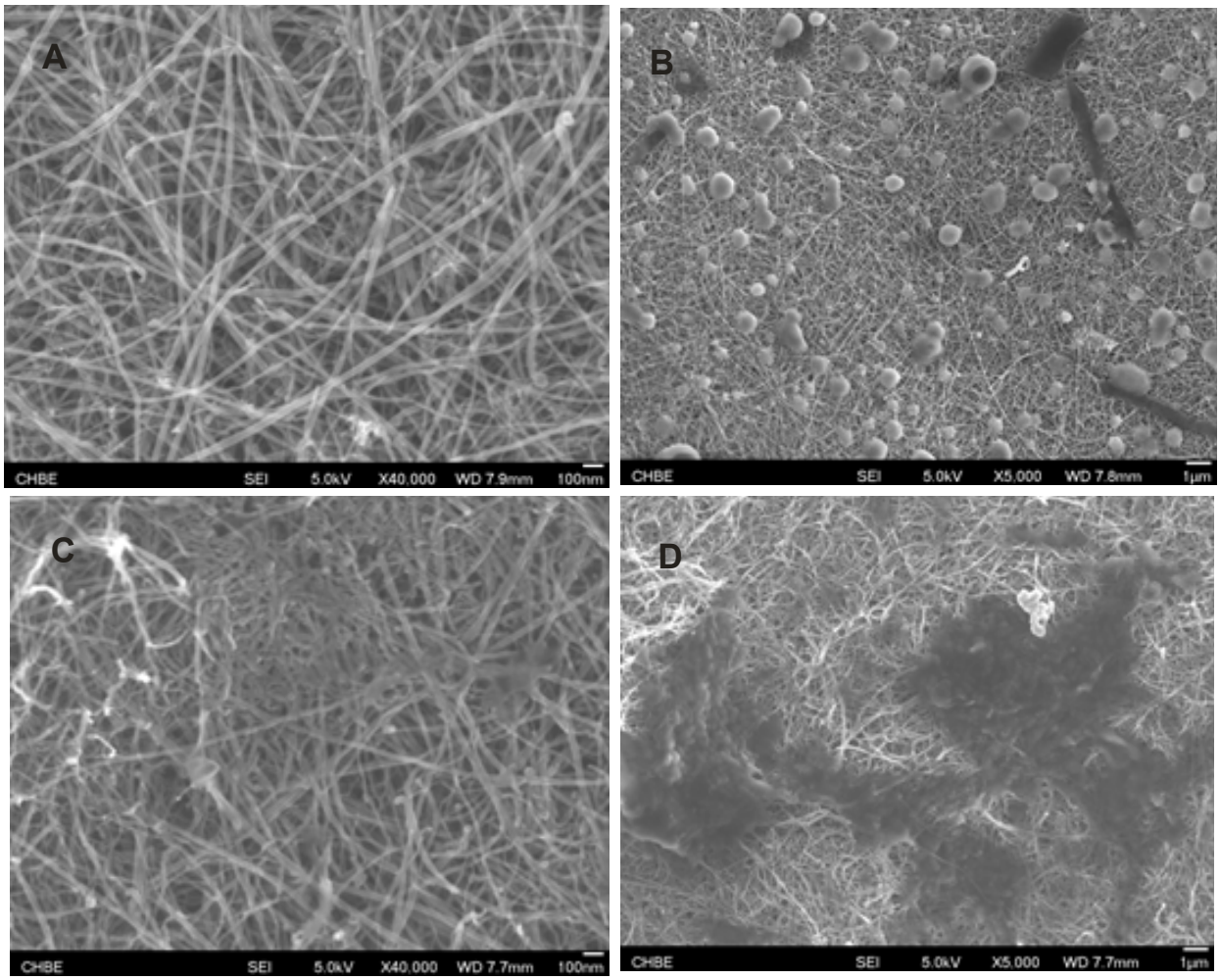

Figure S14. FESEM images of (A) fresh anode CNT, (B) CNT after 5 h continuous phenol oxidation at -0.1 V vs. Ag/AgCl, (C) CNT after 5 h continuous phenol oxidation at -0.4 V vs. Ag/AgCl, and (D) CNT after 20 h continuous phenol oxidation at -0.4 V vs. Ag/AgCl.

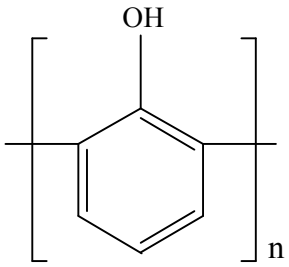

m/z = 91.0189

C_6H_4O

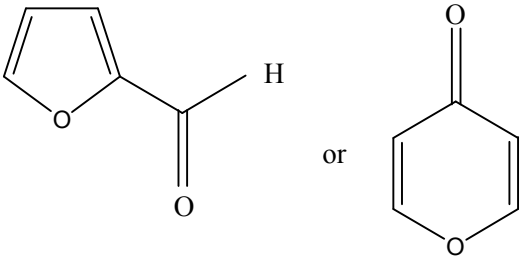

m/z = 95.0137

$C_5H_4O_2$

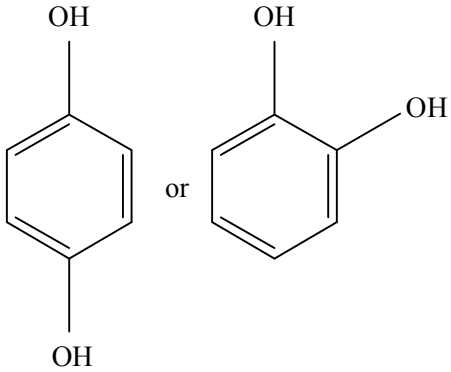

m/z = 109.0294

$C_6H_6O_2$

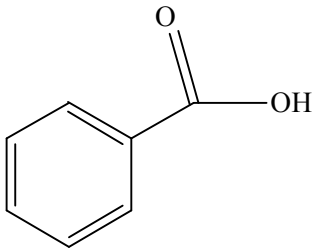

m/z = 121.0294

$C_7H_6O_2$

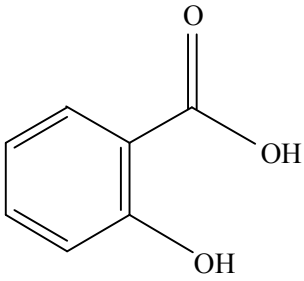

m/z = 137.0243

$C_7H_6O_3$

Figure S15. Representative phenol electrooxidation products. Experimental conditions: [Na_2SO_4] = 10 mmol L^{-1}, phenol flux = 2.20 mol L^{-1} m^{-2}, influent DO flux = 2.20 mol L^{-1} m^{-2}, flow rate = 1.5 mL min^{-1}.

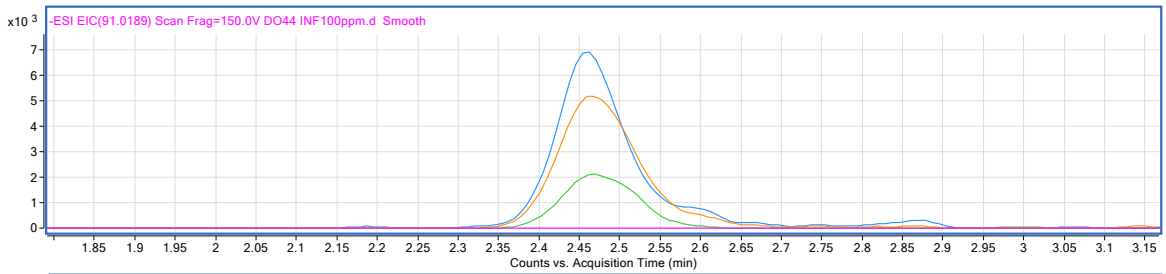
x10 3
-ESI EIC(91.0189) Scan Frag=150.0V DO44 INF100ppm.d Smooth
Counts vs. Acquisition Time (min)

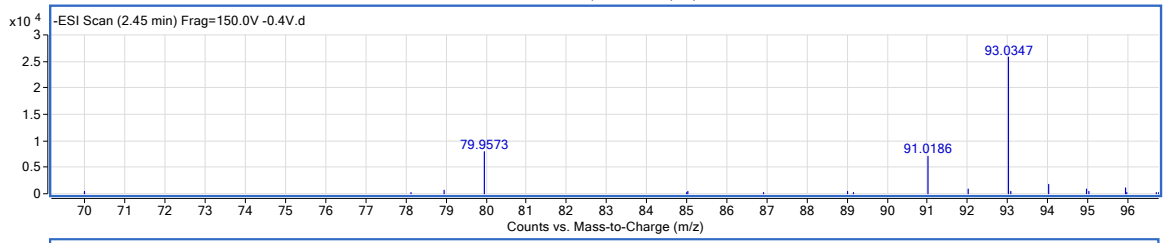
x10 4
-ESI Scan (2.45 min) Frag=150.0V -0.4V.d
93.0347
79.9573
91.0186
Counts vs. Mass-to-Charge (m/z)

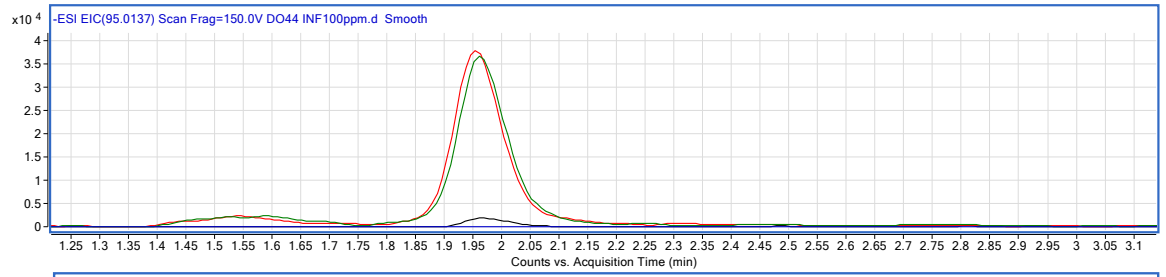
x10 4
-ESI EIC(95.0137) Scan Frag=150.0V DO44 INF100ppm.d Smooth
Counts vs. Acquisition Time (min)

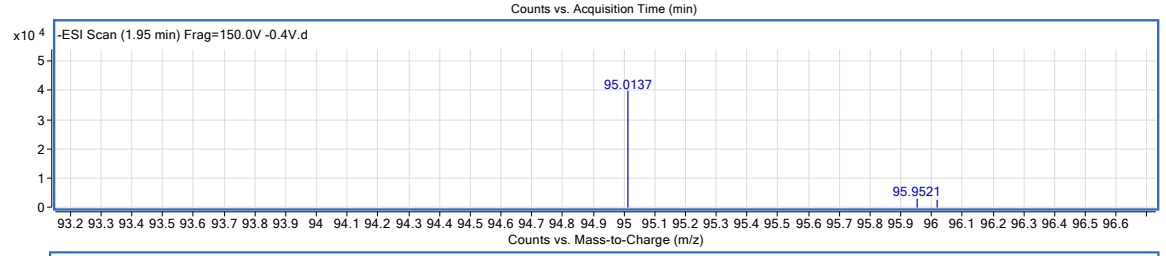
x10 4
-ESI Scan (1.95 min) Frag=150.0V -0.4V.d
95.0137
95.9521
Counts vs. Mass-to-Charge (m/z)

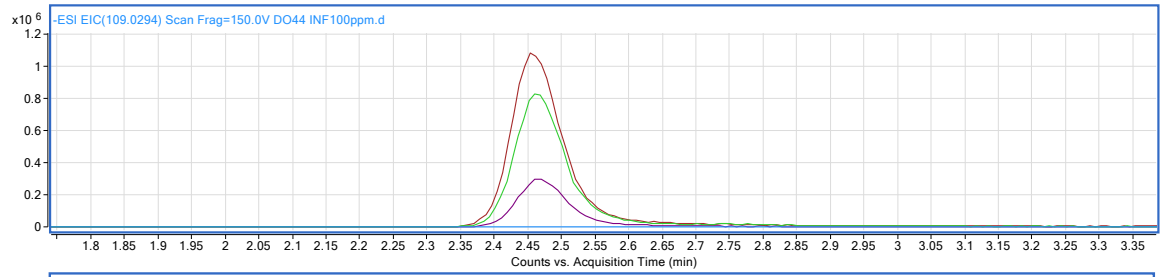
x10 6
-ESI EIC(109.0294) Scan Frag=150.0V DO44 INF100ppm.d
Counts vs. Acquisition Time (min)

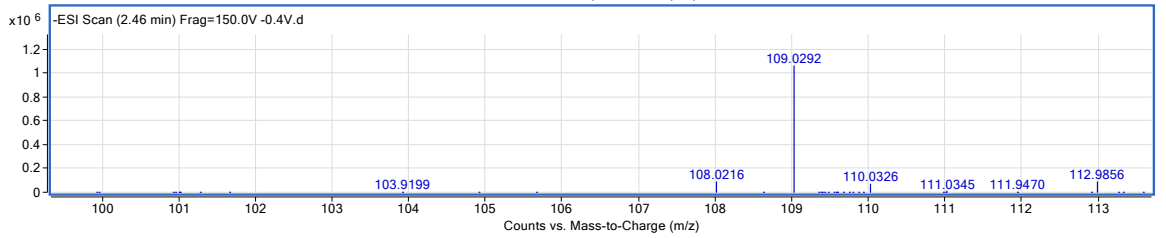
x10 6
-ESI Scan (2.46 min) Frag=150.0V -0.4V.d
109.0292
103.9199
108.0216
110.0326
111.0345
111.9470
112.9856
Counts vs. Mass-to-Charge (m/z)

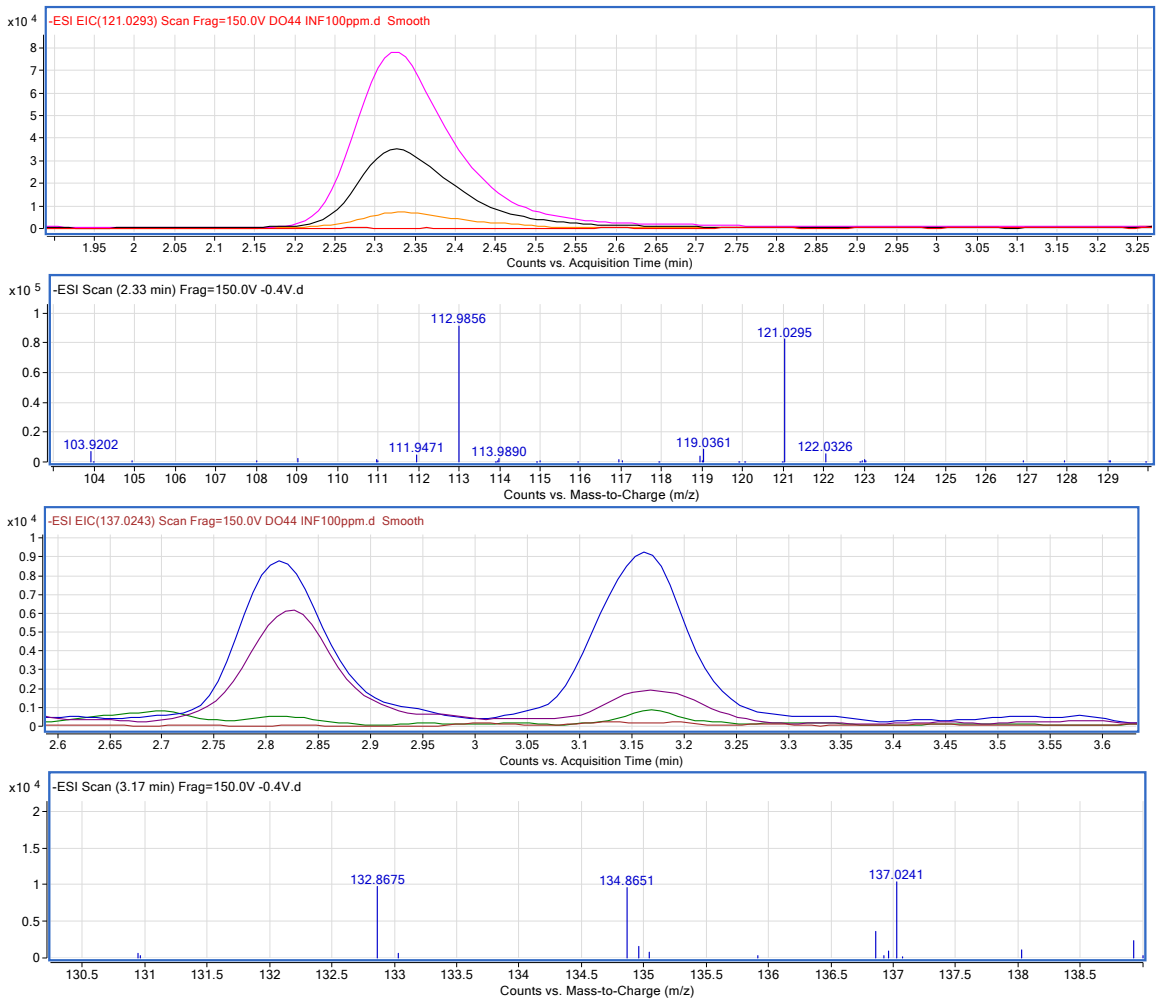

Figure S16. Comparison of the extracted ion chromatogram and mass spectrum of phenol byproducts at applied cathode potential of -0.1, -0.4 and -0.7 V vs. Ag/AgCl: m/z = 91.0189, m/z = 95.0.37, m/z =109.0294, m/z = 121.0293 and m/z = 137.0243.

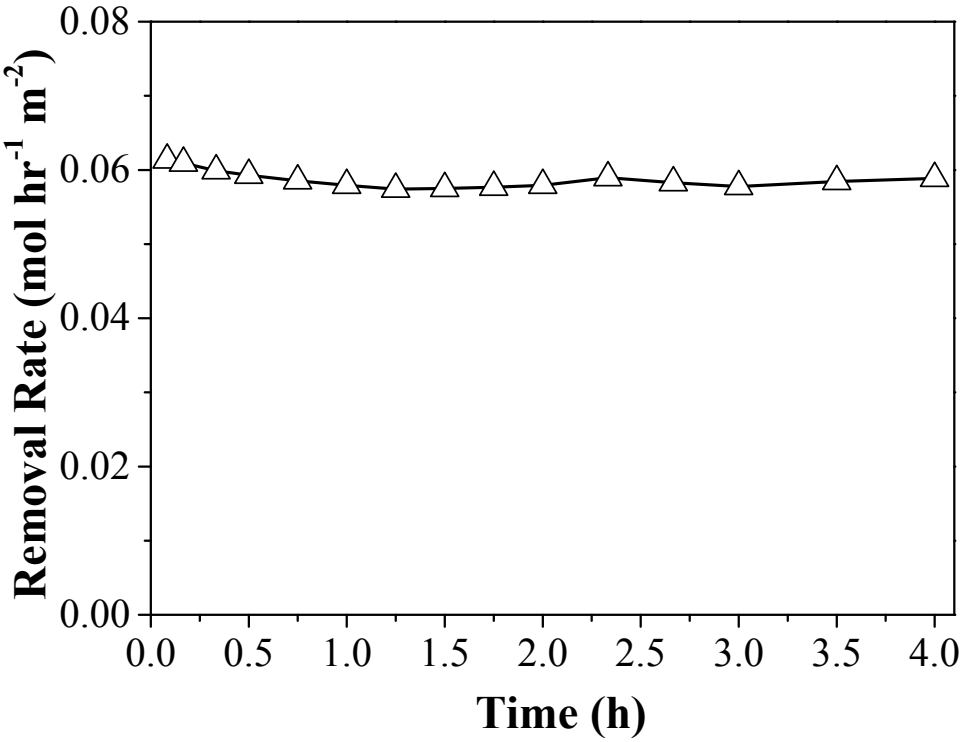

Figure S17. Phenol oxidation rates a function of time. Experimental conditions: phenol flux = 2.20 mol L^{-1} m^{-2}, DO flux = 1.95 mol L^{-1} m^{-2}, applied cathode potential = -0.4 V vs. Ag/AgCl, [Na_2SO_4] = 10 mmol L^{-1}, flow rate = 1.5 mL min^{-1}.

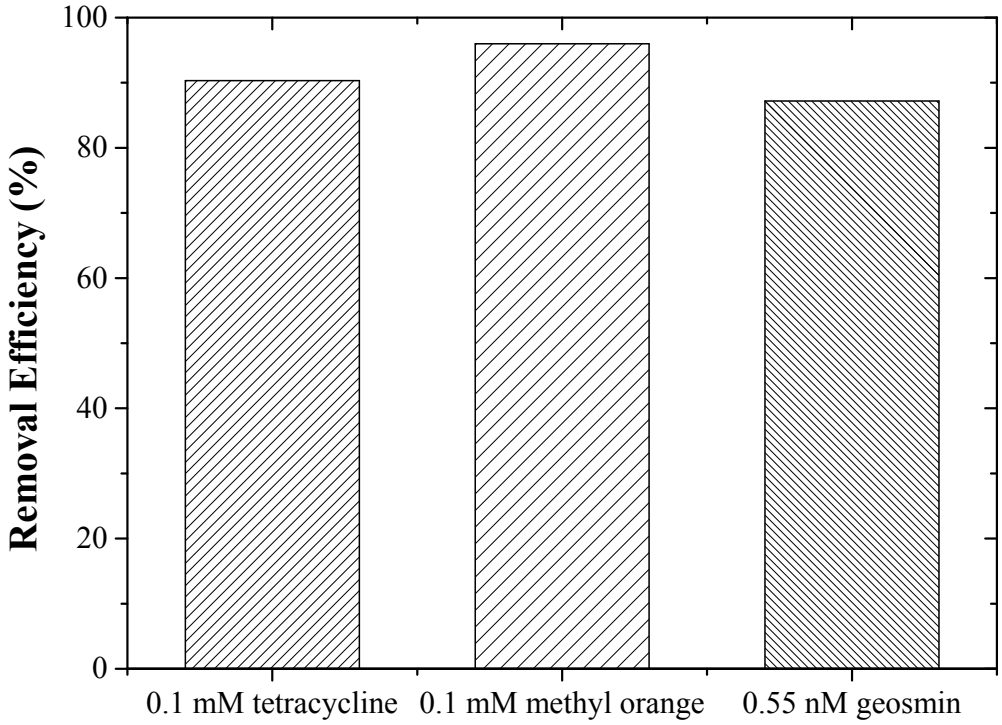

Figure S18. Comparison of removal efficiency of 0.1 mmol L^{-1} tetracycline, 0.1 mmol L^{-1} methyl orange and 0.55 nmol L^{-1} geosmin by the electrochemical filtration system. Experimental conditions: applied cathode potential = -0.4 V vs. Ag/AgCl, [Na_2SO_4]= 10 mmol L^{-1}, influent DO flux = 1.95 mol L^{-1} m^{-2}, and flow rate = 1.5 mL min^{-1}.

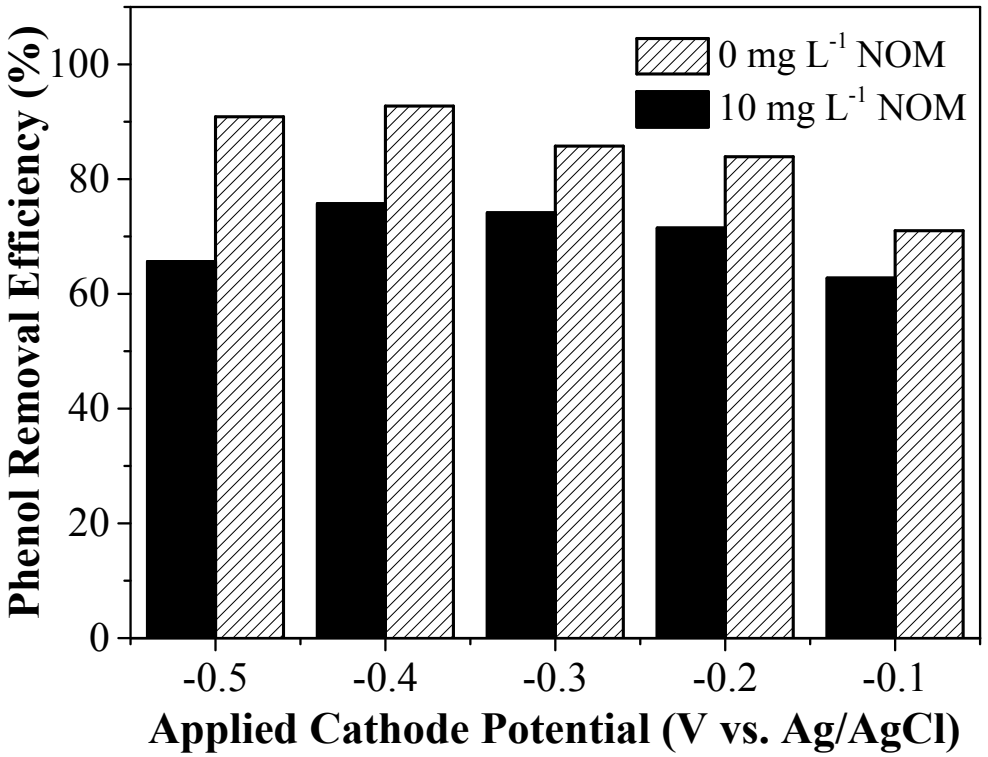

Figure S19. Comparison of phenol removal efficiency as a function of NOM and applied cathode potential. Experimental conditions: Influent phenol = 0.01 mmol L^{-1}, [Na_2SO_4] = 10 mmol L^{-1}, influent DO flux = 1.95 mol L^{-1} m^{-2}, flow rate = 1.5 mL min^{-1}.

A low concentration of phenol (0.01 mmol L^{-1}) was also effectively removed in the filtration system with removal efficiencies ranging between 71.0% and 92.7%, but the presence of 10 mg L^{-1} NOM significantly decreased phenol removal efficiencies to between 62.8% and 74.1%, which was possibly caused by the competition for CNT sorption & electrooxidation sites. These results demonstrated the potentials of coupling *in situ* generated H_2O_2 with CNT electrochemical filtration for environmental applications and further experiments are needed to optimize the electrochemical filtration process under the impacts of NOM and to remove other recalcitrant organic contaminants.

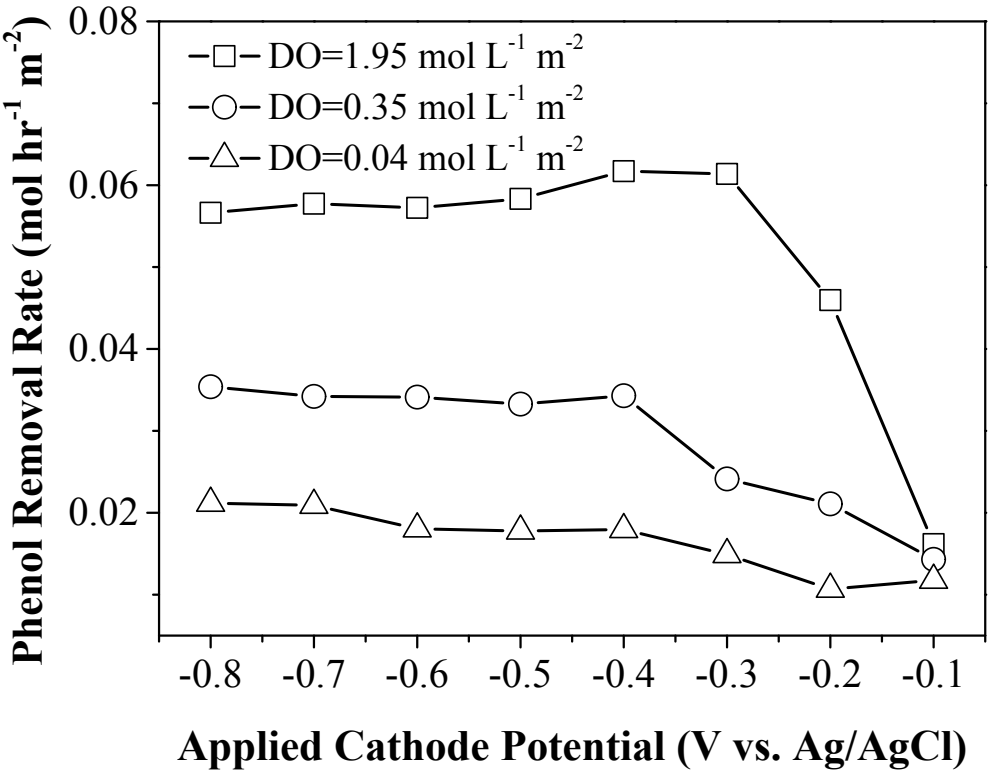

Figure S20. Phenol removal kinetics as a function of applied cathode potential and influent DO flux with 10 mM NaCl as an electrolyte. Experimental conditions: [NaCl] = 10 mmol L^{-1}, flow rate = 1.5 mL min^{-1}.

To further test phenol removal in more realistic conditions, NaCl was employed as an electrolyte to replace Na_2SO_4, and the results indicate that similar phenol removal rate was obtained under saturated DO conditions (DO flux = 1.95 mol L^{-1} m^{-2}). Under deoxygenated condition (DO flux = 0.04 mol L^{-1} m^{-2}), phenol removal rate with NaCl as an electrolyte was higher than that with Na_2SO_4 as an electrolyte, suggesting that anodic production of aqueous oxidants, such as $Cl_2^{\bullet-}$, may contribute to additional phenol removal.

References

1. Beckett, M. A.; Hua, I., Impact of ultrasonic frequency on aqueous sonoluminescence and sonochemistry. *J. Phys. Chem. A* **2001,** *105*, (15), 3796-3802.
2. Kormann, C.; Bahnemann, D. W.; R., H. M., Photocatalytic production of hydrogen peroxides and organic peroxides in aqueous suspensions of titanium dioxide, zinc oxide, and desert sand. *Environ. Sci. Technol.* **1988,** *22*, (7), 798-806.
3. Plakas, K. V.; Karabelas, A. J.; Sklari, S. D.; Zaspalis, V. T., Toward the Development of a Novel Electro-Fenton System for Eliminating Toxic Organic Substances from Water. Part 1. In Situ Generation of Hydrogen Peroxide. *Industrial & Engineering Chemistry Research* **2013,** *52*, (39), 13948-13956.